ACS APPLIED MATERIALS & INTERFACES

Research Article

www.acsami.org

Hollow Cocoon-Like Hematite Mesoparticles of Nanoparticle Aggregates: Structural Evolution and Superior Performances in Lithium Ion Batteries

Jian Zhu, K. Y. Simon Ng, and Da Deng*

Department of Chemical Engineering and Materials Science, Wayne State University, 5050 Anthony Wayne Dr., Detroit, Michigan 48202, United States

Supporting Information

ABSTRACT: We report the facile, fast, and template-free preparation of hollow α-Fe_2O_3 with unique cocoon-like structure by a one-pot hydrothermal method without any surfactants in a short reaction time of 3 h only. In contrast, typical hydrothermal methods to prepare inorganic hollow structures require 24 h or a few days. Templates and/or surfactants are typically used. The hollow α-Fe_2O_3 nanococoon was thoroughly characterized by field-emission scanning electron microscopy (FESEM), transmission electron microscopy (TEM), and X-ray diffraction (XRD). Ex situ analysis of a series of samples prepared at different reaction times clearly revealed the structural evolution and possible formation mechanism. Superior electrochemical performance in terms of cyclability, specific capacity, and high rate was achieved, which could be attributed to its unique hollow cocoon-like structure. Structural stability was revealed by analyzing the samples after 120 charge−discharge cycles. The unusual structural stability of the hollow α-Fe_2O_3 nanococoons after 120 cycles, which is rarely observed for transition metal oxides of particle aggregates, will guarantee further research investigation. Experimental evidence further demonstrated that hollow nanococoons exceed solid nanococoons in reversible lithium-ion storage.

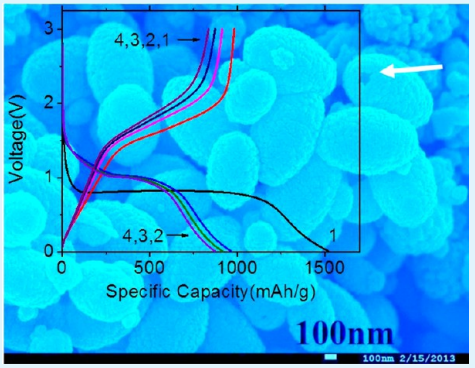

KEYWORDS: *α-Fe_2O_3, hollow cocoons, nanoparticle aggregates, energy storage, lithium, capacity*

1. INTRODUCTION

Rechargeable lithium-ion batteries (LIBs) are currently the dominant power sources for portable electronic devices. The market of LIBs is expanding into electric vehicles and green energy grids. After 20 years of development since the first commercialization of LIBs by Sony in 1991, carbon is still exclusively used as anode materials in LIBs. However, the theoretical capacity of graphite (372 mA h g^{-1} based on LiC_6) is almost achieved, and it becomes one of the bottlenecks to further increase energy density of LIBs based on carbon. Therefore, there is an urgent need to develop carbon-alternative materials with higher capacity to meet the increasing demand for energy storage. Transition metal oxides receive increasing attention as carbon-alternatives because of their much higher theoretical capacity based on a different storage mechanism of conversion and alloying.[1−5] In particular, α-Fe_2O_3 with a theoretical capacity of 1007 mA h g^{-1} has been attracting much attention as a promising candidate to replace carbon.[6−12]

Compared to other transition metal oxide candidates (such as NiO, CoO),[5] α-Fe_2O_3 is outstanding in terms of low cost, abundance, and environmental benignity. However, poor cyclability, a common problem among transition metal oxides, caused by a volume change during the insertion/extraction of Li ions and poor conductivity, is the main challenge. One strategy is to design and tailor α-Fe_2O_3 nanostructures to address the challenge. For example, nanostructured Fe_2O_3 in the form of nanotubes,[13] rods,[14−16] spheres,[17−19] cubes,[20,21] spindles,[22−24] flakes,[25] hollow structures,[23,26−31] and composites[32] has been synthesized for LIBs and achieved a certain degree of success. Particularly, hollow nanostructures are of great interest as the hollow space can accommodate the large volume expansion during Li insertion.[23,27−31] It is always practically interesting and intellectually challenging to develop facile methods to prepare Fe_2O_3 with unique hollow nanostructures.[33−36]

Herein, we report a facile one-pot preparation of hollow α-Fe_2O_3 with unique cocoon-like structure. The size of the hollow nanococoons are about 800 nm in length and 500 nm in diameter. Furthermore, the nanococoons are constructed by aggregation of subunits of nanoparticles about 35 nm in size. Electrochemical evaluation demonstrates that the hollow nanococoons have superior performances in lithium ion storage in terms of capacity, cyclability, and high rate. Results show that

Received: December 5, 2013
Accepted: January 27, 2014
Published: January 27, 2014

   dx.doi.org/10.1021/am4055996 | ACS Appl. Mater. Interfaces 2014, 6, 2996−3001

hollow nanococoons perform better than nonhollow nanococoons.

2. EXPERIMENTAL SECTION

Materials Preparation and Characterization. All the chemicals were used as received. In a typical procedure, a solution of 0.4 mmol of $FeCl_3 \cdot 6H_2O$ dissolved in 16 mL of water was added into another solution of 0.4 mmol of dimethyl oxalate dissolved in 16 mL of 1-propanol drop by drop under stirring. The mixture was then transferred to a 45 mL Teflon-lined autoclave and heated at 200 °C for 3 h. Hollow and solid nanococoons were obtained at 3 h and 75 min of reaction, respectively. The solid products were collected by centrifugation, washed repeatedly with water and ethanol, and dried in a vacuum oven. All samples were fully characterized by field-emission scanning electron microscopy (FESEM) on a JEOL JSM-7600 operating at 15 kV, by transmission electron microscopy and selected area electron diffraction (TEM/SAED) on a JEOL JEM-2010 operating at 200 kV, and by powder X-ray diffraction (XRD) on a Rigaku Smartlab X-ray diffractometer using Cu Kα radiation.

Electrochemical Measurements. Typically, 80 wt % powder of α-Fe_2O_3 nanococoons constructed by aggregated subunits of nanoparticles was mixed with 10 wt % of conductivity enhancer (Super-P carbon black, Timcal) and 10 wt % of polyvinylidene fluoride (PVDF) binder in *N*-methylpyrrolidone (NMP) to form a homogeneous slurry. The slurry was then applied to a copper disc current collector and dried in a vacuum oven. Electrochemical test cells were assembled in an argon-filled glovebox using the coated copper disc as the working electrode, lithium metal as the counter/reference electrode, and 1 M solution of $LiPF_6$ in a 50:50 v/v mixture of ethylene carbonate (EC) and diethyl carbonate (DEC) as the electrolyte. The Swagelok-type cells were charged and discharged galvanostatically at room temperature in the 0.01−3 V voltage window at different C rates on a MTI BST8-WA battery tester.

3. RESULTS AND DISCUSSION

The chemical composition and phase purity of the hollow nanococoons of α-Fe_2O_3 from the one-pot synthesis were confirmed by XRD (Figure 1). All the diffraction peaks can be assigned to α-Fe_2O_3 (JCPDS card no. 33-0664). No other impurities are observed. The diffraction peak (110) is used to estimate the crystalline size calculated from the Scherrer equation and it is about 34 nm. The optical color of the as-prepared powder of hollow nanococoons in a mortar (the inset of Figure 1) is the typical red color of α-Fe_2O_3.[37] The

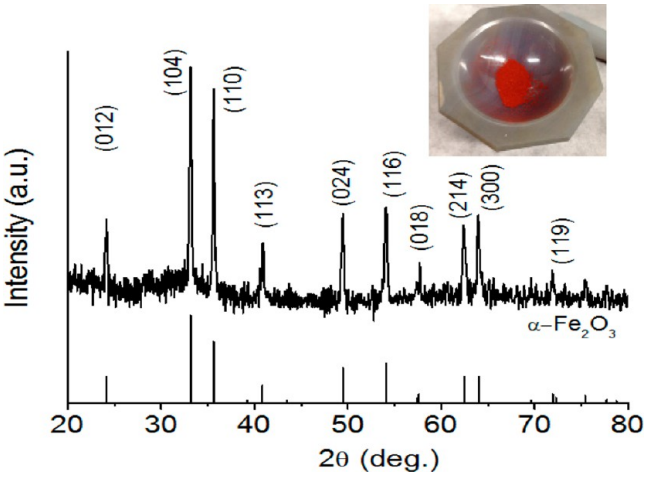

Figure 1. XRD pattern of as-prepared hollow α-Fe_2O_3 nanococoons with building units of nanoparticles; the inset shows the optical image of the red colored α-Fe_2O_3 in a mortar.

successful preparation of α-Fe_2O_3 is also confirmed by EDS (Figure S1, Supporting Information), and the atomic ratio of Fe/O is comparable to commercial α-Fe_2O_3.

The morphology of the unique hollow cocoon-like nanostructures was characterized by both FESEM and TEM images (Figure 2). The low-magnification FESEM image

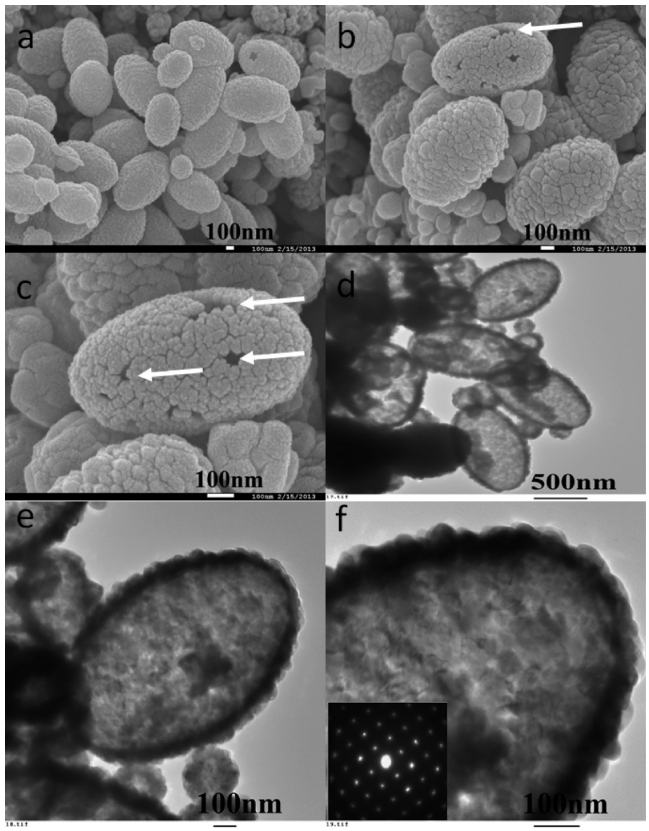

Figure 2. FESEM images of the hollow cocoon-like nanostructures: (a) low-magnification overall view; (b) high-magnification view of a few typical nanococoons; (c) zoom-in view of a typical nanococoon with holes on the broken shell revealing its hollow structure. TEM images of nanococoons: (d) low-magnification overall view; (e) high-magnification view of a typical nanococoon; (f) zoom-in view of a section of the nanococoon revealing the building units of nanoparticles; inset of (f) is the SAED pattern.

(Figure 2a) shows that the as prepared nanoparticles are in the shape of cocoons about 800 nm in length and about 500 nm in diameter. The high-magnification FESEM image (Figure 2b) shows several typical nanococoons. The surface of the nanococoons is rough, indicating the nanococoons are formed by aggregation of subunits of α-Fe_2O_3 nanoparticles. Close examination shows that there are a few holes with size about 50 nm as highlighted by white arrows on the surface of the nanococoons (Figure 2b,c). The presence of holes indicates that the nanococoon is hollow and the shell is formed by assembly of nanoparticles at a size of about 35 nm as building subunits, close to the crystalline size estimated by XRD. The hollow structure generally observed was further confirmed by TEM (Figure 2d). The high-magnification TEM image (Figure 2e) of a typical nanococoon shows clear contrast between the shell and the interior, indicating hollow structure was formed. Furthermore, the zoom-in cross-section view of the shell (Figure 2f) reveals that the shell is not smooth and is about 75 nm in thickness, and it once again confirms the rough shell is

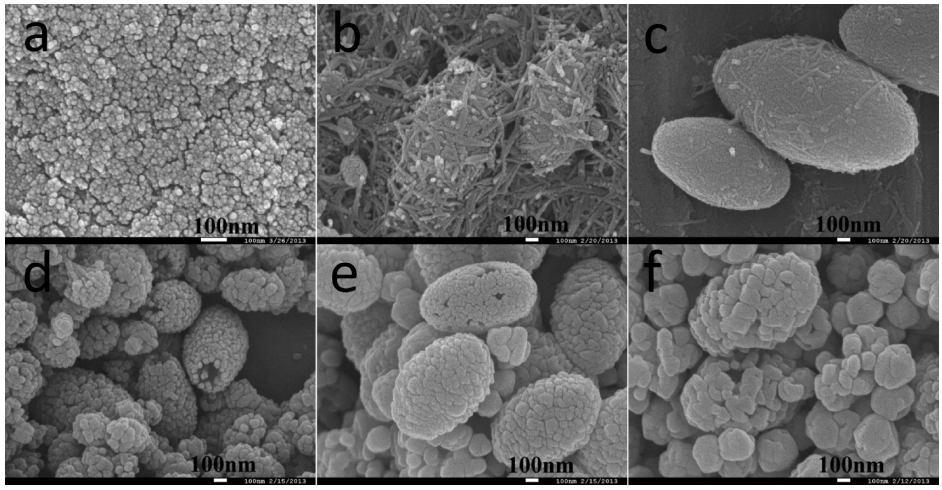

Figure 3. Effect of reaction time: FESEM images of the products obtained after different times of reaction at (a) 15 min, (b) 30 min, (c) 60 min, (d) 75 min, (e) 3 h, and (f) 6 h.

constructed by assembled nanocrystals. The subunits are single crystalline rhombohedral phase of hematite α-Fe_2O_3 as confirmed by selected area electron diffraction (SAED) with sharp diffraction spots (inset of Figure 2f).

To gain a fundamental understanding of the possible mechanism of formation for the unique hollow cocoon-like nanostructures, products obtained under different experimental conditions were thoroughly characterized by FESEM and TEM. Due to limitation of the hydrothermal reaction system with a sealed reactor under high pressure and high temperature, it is hard to monitor the formation of the nanostructures in situ. Therefore, ex situ analysis was carried out for a set of experiments with different reaction time. FESEM images of the particles obtained from different reaction times clearly reveal the growth and evolution from tiny nanoparticles to hollow nanococoons (Figure 3a–f). Nanoparticles about 10 nm in size without any high-order structure were observed after 15 min (Figure 3a), indicating the initial stage of nucleation. When the reaction time was prolonged to 30 min, both nanorods and the sprouts of nanococoons covered with nanorods were observed (Figure 3b). TEM analysis shows that the sprouts of nanococoons were formed by nanorods assembly and were solid (Figure S2a,b, Supporting Information). When the reaction time was increased to 60 min, nanococoons were more mature and no nanorods were left (Figure 3c). When the reaction time was further increased to 75 min, the nanococoons started to form porous structures (Figures 3d and S2c,d, Supporting Information). When the reaction time was 3 h, the nanococoons turned hollow as evidenced by broken holes on the surface of nanococoons (Figure 3e) and TEM (Figure S2e,f, Supporting Information). It is interesting to observe the transition from solid to hollow structure as direct evidence for the possible Ostwald Ripening mechanism. Furthermore, the subunits which aggregate to form nanococoons grew larger when reaction time was increased from 3 to 6 h. The effect of dimethyl oxalate on the morphology was explored as well (Figure S3, Supporting Information). With a smaller amount of dimethyl oxalate at 0.2 mmol, hollow nanospheres with a diameter of ~800 nm formed rather than nanococoons (Figure S3a,b, Supporting Information). Only when the amount was increased to 0.4–0.8 mmol were hollow nanococoons observed (Figure S3c–f, Supporting Information). This indicates the important role of oxalate ions released from decomposition of dimethyl oxalate in guiding the formation of the nanococoons.

On the basis of the experimental observation, a plausible formation mechanism is proposed and illustrated in Figure 4a.

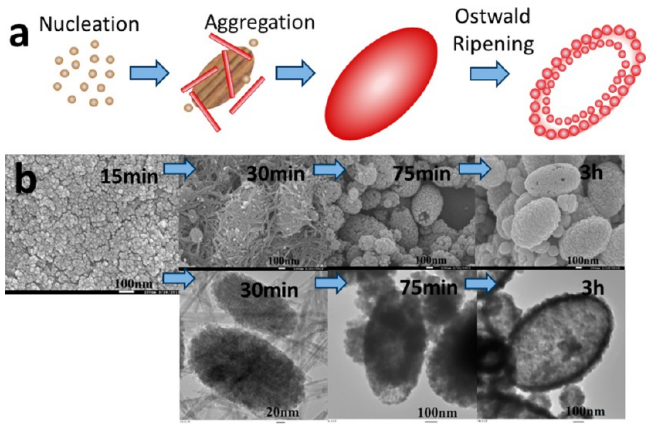

Figure 4. (a) Illustration of the proposed formation mechanism for hollow nanococoons; (b) ex situ electron microscope images for samples prepared from 15, 30, 75 min, and 3h of reaction and the reaction time is labeled in each corresponding FESEM (top) and TEM (bottom) images.

Once precipitation occurs, tiny colloids form first by nucleation generating tiny nanoparticles (Step 1). With the linear guiding property of oxalate ions released from dimethyl oxalate toward cations, nanorods are formed. During this stage, the newly produced nanorods possess high surface energy and tend to aggregate to form nanococoons to minimize surface energy of the system (Step 2 and 3). The formation of voids in the nanococoons is likely due to the Ostwald ripening mechanism as evidenced experimentally. The inner core area has higher surface energy due to aggregation of smaller primary units at an early stage and is easily dissolved as compared to the external shells. Ostwald ripening is strongly dependent on interfacial energy, crystal growth rate, and equilibrium solubility.[38] During the ripening process, the low-density cores are dissolved and are redistributed to surfaces to minimize energy. Therefore, hollow structures are formed. Figure 4b summarized the electron microscope characterization of the particles at the

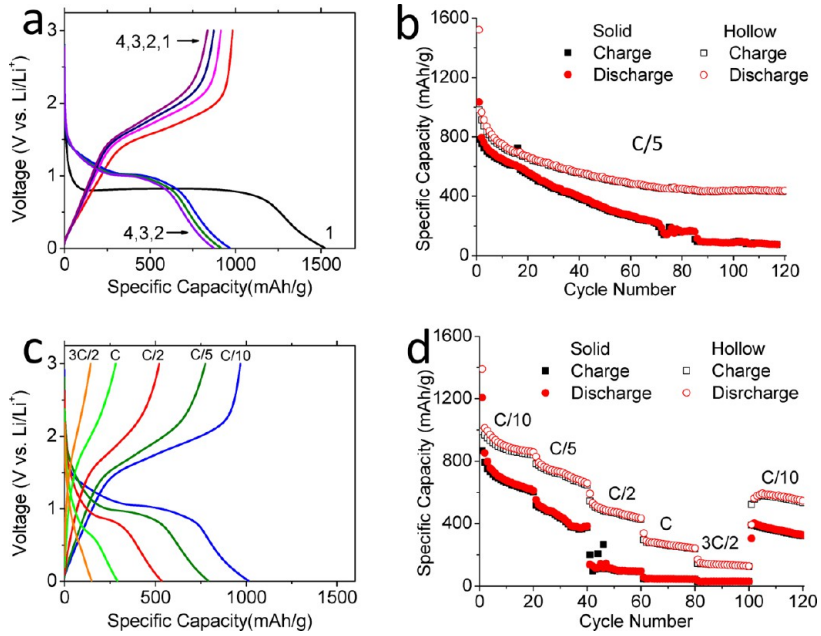

Figure 5. (a) First 4 cycles of charge−discharge profiles of hollow nanococoons; (b) capacity vs cycle number plots of hollow and solid nanococoons at C/5 rate; (c) charge−discharge profiles at different current rates of C/10, C/5, C/2, C, and 3C/2 for one cell. (d) Rate performance of hollow vs solid nanococoons.

corresponding stage of formation, matching well with the illustration. However, further work is underway to obtain more details on the mechanism of formation.

To demonstrate their potential application as anode materials for LIBs, hollow nanococoons of α-Fe_2O_3 were electrochemically evaluated in Swagelok testing cells. The first four cycles of charge−discharge profiles obtained at C/5 rate (1C = 1000 mA g^{-1}) are plotted in Figure 5a. The charge and discharge voltage plateaus are typical for α-Fe_2O_3 as reported in the literature.[19] The first cycle discharge (lithiation) and charge (delithiation) capacities are 1521 and 983 mA h g^{-1}, respectively. The 35% first cycle capacity loss can be attributed to the electrochemical reduction of Fe_2O_3 and decomposition of the electrolyte and formation of solid electrolyte interphase (SEI). The hollow structure formed by aggregation of subunits with large surface area would lead to nearly complete reduction reaction from Fe^{3+} to Fe^0 in the first cycle.[39] It is interesting to note that the plateau at around 1.2 V contributing 300 mA h g^{-1} observed by Reddy et al.[9] and 1.58 V by Zhou et al.[12] is weak here. On the other hand, the plateau at ~0.75 V is dominant contributing 1200 mA h g^{-1} which may be assigned to the reduction of Fe ions to nanoscale Fe^0 metal and the formation of Li_2O. The slight difference observed in first cycle discharge profiles among α-Fe_2O_3 nanoflakes,[9] nanotubes,[39] multishelled hollow spheres,[12] and hollow nanococoons reported here suggests that the morphology of the nanoscale α-Fe_2O_3 may play a significant role in determining the discharge characteristics, which requires further studies. The voltage drop from below 0.75 to 0.01 V may be attributed to the formation of a solid electrolyte interphase (SEI) and decomposition of the solvent in the electrolyte.[9] The first cycle charge profile is similar to the second onward cycle charge profiles suggesting the same electrochemical reaction involved. The reaction could involve the decomposition of Li_2O with assistance of nanostructured metallic iron (Fe^0).[9] The similarity in second cycle discharge profile and those subsequent cycles suggests the electrochemical reaction is highly reversible.

The electrochemical reactions involved could be the following:[9,39,40]

$$Fe_2O_3 + 2Li^+ + 2e^- \Rightarrow Li_2(Fe_2O_3) \quad (1)$$

$$Li_2(Fe_2O_3) + 4Li^+ + 4e^- \Rightarrow 2Fe^0 + 3Li_2O \quad (2)$$

$$2Fe^0 + 2Li_2O \leftrightharpoons 2Fe^{II}O + 4Li^+ + 4e^- \quad (3)$$

The cyclability was evaluated with prolong cycling test over 120 cycles at current rate of 200 mA g^{-1} (Figure 5b, hollow). The capacity of 437 mA h g^{-1} at 120th cycle is still 25% higher than that of commercial graphite with useful capacity of 350 mA h g^{-1}. Compared to micro α-Fe_2O_3 which faded to negligible capacity within 10 cycles,[41] the hollow nanococoons demonstrated significantly improved cycling performance over 120 cycles. Furthermore, rate performance of hollow nanococoons is also superior over those solid nanococoons (Figure 5d, hollow vs solid). The hollow nanococoons show comparable electrochemical performance to hollow spindles and hollow spheres reported.[23] On the other hand, the voltage plateaus and changes in the charge−discharge profiles are the same in both hollow and solid α-Fe_2O_3 nanococoons (Figure S4, Supporting Information), indicating the same electrochemical reactions involved, as expected. These results suggest the important role of hollow structure in improving performance in reversible lithium ion storage. The superior electrochemical performance could be attributed to the hollow interior and porous shell structure of the nanococoon with building subunit aggregation. The unique structures can accommodate the volume change during the charge/discharge process and provide shorter distance for transportation of Li^+ ions. Furthermore, a high coulombic efficiency of 99% was achieved from 2nd cycle to 120th cycle.

The rate performance of the hollow nanococoons was evaluated by charging/discharging the cells at different current density from C/10, C/5, C/2, C, 1.5C, and back to C/10 for 20 cycles interval each (Figure 5c,d). The charge−discharge

dx.doi.org/10.1021/am4055996 | ACS Appl. Mater. Interfaces 2014, 6, 2996−3001

profiles of the 2nd, 22nd, 42nd, 62nd, and 82nd cycles tested at C/10, C/5, C/2, C, and 1.5C, respectively, were plotted in Figure 5c. Specific capacities of 1013, 791, 534, 290, and 149 mA h g^{-1} were achieved at the corresponding current rates. It is particularly interesting to note that the capacity jumps back to 563 from 149 mA h g^{-1} when the current rate is reassumed to 100 mA g^{-1} from 1500 mA g^{-1} (Figure 5d, hollow). The results suggest that the electrode materials can sustain the extensive cycling at high rates, which is desirable. In fact, overall morphology of the nanocoons was well preserved after 120 cycles as revealed by FESEM images of the electrode disassembled after the cycling test (Figure 6a–d). The high-

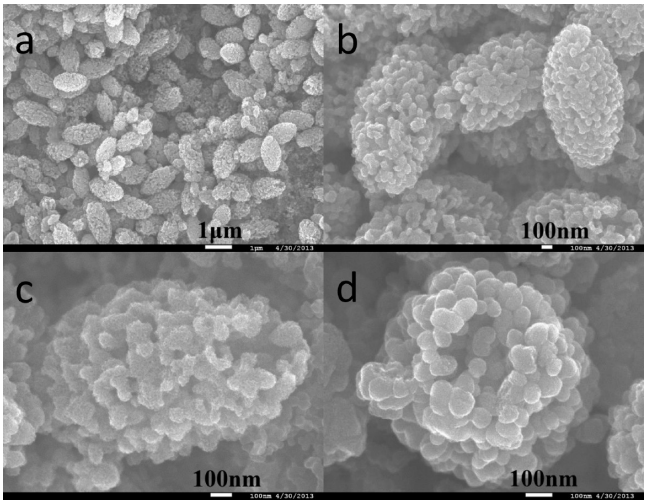

Figure 6. FESEM images of electrode after the 120 cycles of test reveal the well maintained overall morphology of cocoon-like structure with high porosity and hollow nature and construction by building units (a) low-magnification view; (b) high-magnification view of few typical nanococoons; (c) zoom-in view of typical nanococoons with broken end revealing its hollow nature; (d) top-view of the broken tip.

magnification images (Figure 6c,d) clearly show that the size of the building units increased to about 100 nm, and the nanoporous nature is maintained. Furthermore, hollow structure is also preserved as observed from those broken nanococoons, and the hollow core part is shrunk due to the enlarged building subunits (Figure 6). The unusual structural stability of the α-Fe_2O_3 nanococoons after 120 cycles, which is rarely observed for transition metal oxides of particle aggregates upon extensive cycling, will guarantee further investigation.

4. CONCLUSIONS

A novel facile template-free one-pot synthesis procedure for the preparation of hollow nanococoons α-Fe_2O_3 assembled by aggregation of subunits of nanoparticles was developed. The formation mechanism was revealed by ex situ analysis of the samples prepared from different times of reaction. Improved electrochemical performance in terms of cyclability, specific capacity, and high rate was achieved. Structure stability was exhibited by the analysis of the samples after 120 cycles. Experimental evidence clearly shows that hollow nanococoons are superior over solid nanococoons in reversible lithium ion storage.

■ ASSOCIATED CONTENT

Supporting Information

EDS results to confirm the chemical composition of the iron oxides product; ex-situ TEM characterization of α-Fe_2O_3 prepared at different times; FESEM images to show the effect of amount dimethyl oxalate on morphology; charge–discharge profiles for both solid and hollow nanococoons. This information is available free of charge via the Internet at http://pubs.acs.org/.

■ AUTHOR INFORMATION

Corresponding Author

*E-mail: da.deng@wayne.edu.

Notes

The authors declare no competing financial interest.

■ REFERENCES

(1) Poizot, P.; Laruelle, S.; Grugeon, S.; Dupont, L.; Tarascon, J. *Nature* **2000**, *407*, 496.
(2) Aricò, A. S.; Bruce, P.; Scrosati, B.; Tarascon, J.-M.; Van Schalkwijk, W. *Nat. Mater.* **2005**, *4*, 366.
(3) Bruce, P. G.; Scrosati, B.; Tarascon, J. M. *Angew. Chem., Int. Ed.* **2008**, *47*, 2930.
(4) Lou, X. W. D.; Archer, L. A.; Yang, Z. *Adv. Mater.* **2008**, *20*, 3987.
(5) Poizot, P.; Laruelle, S.; Grugeon, S.; Dupont, L.; Tarascon, J. M. *Nature* **2000**, *407*, 496.
(6) Ban, C. M.; Wu, Z. C.; Gillaspie, D. T.; Chen, L.; Yan, Y. F.; Blackburn, J. L.; Dillon, A. C. *Adv. Mater.* **2010**, *22*, E145.
(7) Chen, J.; Xu, L. N.; Li, W. Y.; Gou, X. L. *Adv. Mater.* **2005**, *17*, 582.
(8) Hu, X. L.; Yu, J. C.; Gong, J. M.; Li, Q.; Li, G. S. *Adv. Mater.* **2007**, *19*, 2324.
(9) Reddy, M. V.; Yu, T.; Sow, C. H.; Shen, Z. X.; Lim, C. T.; Rao, G. V. S.; Chowdari, B. V. R. *Adv. Funct. Mater.* **2007**, *17*, 2792.
(10) Wu, C. Z.; Yin, P.; Zhu, X.; OuYang, C. Z.; Xie, Y. *J. Phys. Chem. B* **2006**, *110*, 17806.
(11) Zhu, X. J.; Zhu, Y. W.; Murali, S.; Stollers, M. D.; Ruoff, R. S. *ACS Nano* **2011**, *5*, 3333.
(12) Zhou, L.; Xu, H.; Zhang, H.; Yang, J.; Hartono, S. B.; Qian, K.; Zou, J.; Yu, C. *Chem. Commun.* **2013**, *49*, 8695.
(13) Kang, N.; Park, J. H.; Choi, J.; Jin, J.; Chun, J.; Jung, I. G.; Jeong, J.; Park, J.-G.; Lee, S. M.; Kim, H. J.; Son, S. U. *Angew. Chem., Int. Ed.* **2012**, *51*, 6626.
(14) Zhou, W.; Tang, K.; Zeng, S.; Qi, Y. *Nanotechnology* **2008**, *19*, 065602.
(15) Ganguli, A. K.; Ahmad, T. *J. Nanosci. Nanotechnol.* **2007**, *7*, 2029.
(16) Cho, W.; Park, S.; Oh, M. *Chem. Commun.* **2011**, *47*, 4138.
(17) Jia, X. H.; Song, H. J. *J. Nanopart. Res.* **2012**, *14*, 1.
(18) Cao, S.-W.; Zhu, Y.-J. *J. Phys. Chem. C* **2008**, *112*, 6253.
(19) Wang, B.; Chen, J. S.; Wu, H. B.; Wang, Z.; Lou, X. W. *J. Am. Chem. Soc.* **2011**, *133*, 17146.
(20) Liang, X.; Wang, X.; Zhuang, J.; Chen, Y.; Wang, D.; Li, Y. *Adv. Funct. Mater.* **2006**, *16*, 1805.
(21) Cao, H.; Wang, G.; Warner, J. H.; Watt, A. A. *Appl. Phys. Lett.* **2008**, *92*, 013110.
(22) Xu, X.; Cao, R.; Jeong, S.; Cho, J. *Nano Lett.* **2012**, *12*, 4988.
(23) Zeng, S.; Tang, K.; Li, T.; Liang, Z.; Wang, D.; Wang, Y.; Zhou, W. *J. Phys. Chem. C* **2007**, *111*, 10217.
(24) Ang, W. A.; Gupta, N.; Prasanth, R.; Srinivasan, M. *ACS Appl. Mater. Interfaces* **2012**, *4*, 7011.
(25) Reddy, M.; Yu, T.; Sow, C. H.; Shen, Z. X.; Lim, C. T.; Subba Rao, G.; Chowdari, B. *Adv. Funct. Mater.* **2007**, *17*, 2792.
(26) Chen, J. S.; Zhu, T.; Yang, X. H.; Yang, H. G.; Lou, X. W. *J. Am. Chem. Soc.* **2010**, *132*, 13162.
(27) Wu, Z.; Yu, K.; Zhang, S.; Xie, Y. *J. Phys. Chem. C* **2008**, *112*, 11307.

(28) Kim, H.-J.; Choi, K.-I.; Pan, A.; Kim, I.-D.; Kim, H.-R.; Kim, K.-M.; Na, C. W.; Cao, G.; Lee, J.-H. *J. Mater. Chem.* **2011**, *21*, 6549.
(29) Song, H.-J.; Li, N.; Shen, X.-Q. *Appl. Phys. A: Mater. Sci. Process.* **2011**, *102*, 559.
(30) Hu, C.-Y.; Xu, Y.-J.; Duo, S.-W.; Li, W.-K.; Xiang, J.-H.; Li, M.-S.; Zhang, R.-F. *J. Chin. Chem. Soc.* **2010**, *57*, 1091.
(31) Liu, J.; Li, Y.; Fan, H.; Zhu, Z.; Jiang, J.; Ding, R.; Hu, Y.; Huang, X. *Chem. Mater.* **2009**, *22*, 212.
(32) Zhu, X.; Zhu, Y.; Murali, S.; Stoller, M. D.; Ruoff, R. S. *ACS Nano* **2011**, *5*, 3333.
(33) Sha, G.; Wang, T.; Xiao, J.; Liang, C. *Mater. Res. Bull.* **2004**, *39*, 1917.
(34) An, Z.; Zhang, J.; Pan, S.; Song, G. *Powder Technol.* **2012**, *217*, 274.
(35) Zhu, W.; Cui, X.; Wang, L.; Liu, T.; Zhang, Q. *Mater. Lett.* **2011**, *65*, 1003.
(36) NuLi, Y.; Zhang, P.; Guo, Z.; Liu, H. *J. Electrochem. Soc.* **2008**, *155*, A196.
(37) Katsuki, H.; Komarneni, S. *J. Am. Ceram. Soc.* **2003**, *86*, 183.
(38) Deng, D.; Martin, S. T.; Ramanathan, S. *J. Mater. Res.* **2011**, *26*, 1545.
(39) Chen, J.; Xu, L.; Li, W.; Gou, X. *Adv. Mater.* **2005**, *17*, 582.
(40) Larcher, D.; Bonnin, D.; Cortes, R.; Rivals, I.; Personnaz, L.; Tarascon, J.-M. *J. Electrochem. Soc.* **2003**, *150*, A1643.
(41) Larcher, D.; Masquelier, C.; Bonnin, D.; Chabre, Y.; Masson, V.; Leriche, J.-B.; Tarascon, J.-M. *J. Electrochem. Soc.* **2003**, *150*, A133.